Active control of laminar-turbulent transition using instantaneous vorticity signals at the wall

Christoph Gmelin and Ulrich Rist
Institut für Aerodynamik und Gasdynamik, Universität Stuttgart, Pfaffenwaldring 21, D-70550 Stuttgart, Germany

(Received 21 March 2000; accepted 7 November 2000)

Many approaches with the objective to actively delay the laminar-turbulent transition in boundary layers are currently under investigation. These approaches, which are mostly based on the superposition of anti-phase disturbances, fail in cases where high (nonlinear) disturbance amplitudes occur. One possible solution to overcome this problem is the direct feedback of instantaneous flow signals from the wall. In our case the spanwise vorticity (ω_z) on the wall is sensed, multiplied by a certain factor A and prescribed as a new boundary condition at the wall with some time delay Δt. This procedure (called ω_z-*control*) yields a robust algorithm which is less influenced by nonlinearities than other processes based on the linear superposition of disturbances (waves). The method was developed and evaluated using both linear stability theory and a three-dimensional spatial DNS code solving the complete Navier–Stokes equations. © *2001 American Institute of Physics.* [DOI: 10.1063/1.1336153]

I. INTRODUCTION

The most popular approach controlling transition is the superposition of disturbances with opposite phase to the existing waves. First attempts have been published by Milling,[1] Liepmann *et al.*,[2,3] and Kozlov *et al.*[4] Until now this strategy has been realized many more times both experimentally[5] and numerically.[6] For disturbances with small (linear) amplitude a reduction in amplitude of up to 90% even in experiments is achievable. In contrast to their excellent performance in early transition stages these approaches do not work satisfactory in cases where high amplitudes occur due to nonlinear effects superposing disturbance and control wave. Moreover, the generation of large control waves which are necessary to cancel the initial wave with the aid of a suction/blowing slot sometimes causes very high velocities in the vicinity of these actuators, an effect which favors nonlinearities furthermore. These arguments make clear that there is a need for a smooth, robust control algorithm which is almost independent of the amplitude of the initial disturbance. Several attempts have been made to control turbulent flows. Control via affection of the vorticity flux at the wall has been proposed by Koumoutsakos,[7,8] whereas Choi, Moin, and Kim[9] observed a damping effect on turbulent flows feeding back the instantaneous wall-normal velocity at a certain distance from the wall to the boundary. They report the establishing of a ''virtual wall,'' i.e., a plane that has approximately no through-flow halfway between the detection plane and the wall and therefore a drag reduction of 25% and a strong reduction of turbulent flow structures. In some aspects our approach is very similar to their idea of feedback of instantaneous signals but in most cases flow data of the whole flow field is not available. In our case this problem is handled by sensing the spanwise vorticity at the wall, present as wall shear stress and easily measurable by hot film sensors or cavity hot wires,[10] for example. These signals are multiplied with a certain factor and prescribed as wall-normal velocity v at the wall (for a detailed description see below in Sec. III).

An approach complementary to our LST investigations (Sec. IV) has been applied by Joshi *et al.*[11] for plane Poiseuille flow using the spanwise shear at the wall as sensor variable and blowing/suction for actuation, as well. However, they converted the problem into a control theoretical one and determined the effect of the feedback control by the position of the zeros and poles of the system. Furthermore, they obtained an optimal sensor location relative to the actuator similar to our most effective phase shift between sensing and actuation. Another contribution concerning feedback control, again in planar Poiseuille flow was published by Hu *et al.*[12] Analogical to our approach they modified the Orr–Sommerfeld equation to get some information about the stability of the controlled flow system. In contrast to the actuation via blowing/suction at the wall used in our investigations they modulated the wall temperature periodically to alter the fluid's viscosity and therefore to stabilize the flow.

In our paper we use direct numerical simulations (DNS) and linear stability theory (LST) to explore the concept of ω_z-control and to evaluate its effects on the disturbances involved in the laminar-turbulent transition in a Blasius boundary layer. The DNS method and a discussion of results in the linear regime are presented in Secs. II and III, investigations using LST in Sec. IV, active control of nonlinear disturbances in Sec. V and a summary is given in Sec. VI.

We have to admit the lack of comparison to experimental results but to our knowledge there are not any experiments concerning the direct feedback-control yet. One reason may be the need for a very densely packed sensor/actuator array. Therefore, one future goal will be to study if this ap-

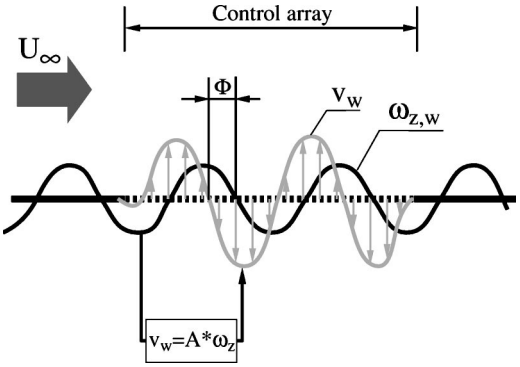

FIG. 1. Illustration of the ω_z-control principle.

proach can be realized by a more sparse sensor/actuator arrangement. In the actual state of affairs we have to agree with the following quotation of Choi *et al.*:[9] ‘‘ *. . . simulations can provide data on what may be possible to achieve just from fluid dynamical considerations. The primary role of simulations in the field of flow control will be to guide experiments for complex flows.*’’

II. NUMERICAL METHOD

All simulations were performed in a rectangular integration domain with the spatial DNS-code developed by Konzelmann, Rist, and Kloker.[13–15] The flow is split into a steady 2D-part (Blasius base flow) and an unsteady 3D-part. The x-(streamwise) and y-(wall-normal) directions are discretized with finite differences of fourth-order accuracy and in the spanwise direction z a spectral Fourier representation is applied. Time integration is performed by the classical fourth-order Runge–Kutta scheme. The utilized variables are normalized with $\tilde{U}_\infty = 30$ m/s, $\tilde{\nu} = 1.5\times 10^{-5}$ m/s^2 and $\tilde{L} = 0.05$ m ($\tilde{}$ denotes dimensional variables):

$$x=\frac{\tilde{x}}{\tilde{L}},\quad y=\frac{\tilde{y}}{\tilde{L}},\quad z=\frac{\tilde{z}}{\tilde{L}},\quad t=\tilde{t}\cdot\frac{\tilde{U}_\infty}{\tilde{L}},$$

$$u=\frac{\tilde{u}}{\tilde{U}_\infty},\quad v=\frac{\tilde{v}}{\tilde{U}_\infty},\quad w=\frac{\tilde{w}}{\tilde{U}_\infty},\quad \mathrm{Re}=\frac{\tilde{U}_\infty\tilde{L}}{\tilde{\nu}}=10^5,$$

where u, v, and w are the components of the unsteady velocity disturbances. This leads to the dimensionless frequency $\beta = 2\pi\tilde{f}\tilde{L}/\tilde{U}_\infty$, where $\tilde{f}$ is the frequency in Hz and the dimensionless spanwise vorticity $\omega_z = (\partial u/\partial y) - (\partial v/\partial x)$.

III. CONTROL MECHANISM

To actively damp disturbances in boundary layers we use the feedback of instantaneous signals of the spanwise vorticity fluctuations measured at the wall. These signals are multiplied by an amplitude factor $|A|$ and are prescribed as a v-boundary condition after a time delay Δt at the wall which is necessary to produce the phase shift Φ shown in Fig. 1. The effects of changing $|A|$ and Δt resp. Φ will be studied in

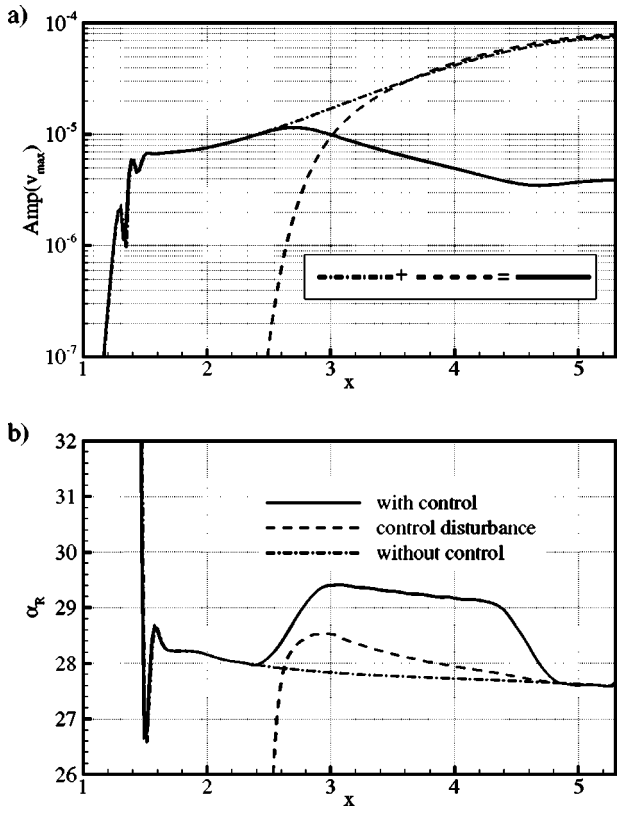

FIG. 2. v-amplitude (a) and wave number (b) of undisturbed linear wave, controlled wave and control disturbance. Control parameters: $|A| = 7.5\times 10^{-5}$, $\Delta t = 0$, control array from $x = 2.4 \ldots 4.8$. Control disturbance is obtained by an extra simulation prescribing the wall signal of the run with control at the wall without initial disturbance. Due to the presence of linear waves addition of modes is valid.

Sec. IV using linear stability theory. Here, results of DNS are analyzed in order to show how the method works in the linear case.

For a small-amplitude 2D Tollmien–Schlichting (TS) wave results of three simulations are compared with each other in Fig. 2. Compared to the uncontrolled case there is a strong damping effect of the ω_z-control on the disturbance amplitude in Fig. 2(a). Because of the small amplitudes a linear superposition of waves is valid here, i.e., the controlled wave (—) in Fig. 2(a) can also be viewed as the addition of the uncontrolled wave (-·-·-·-) with a control wave which arises when previously extracted v_w (index w denotes wall quantities) signals are prescribed in an otherwise undisturbed flow (- - -). However, this approach has to be clearly distinguished from the ‘‘classical’’ wave superposition principle,[5] where an anti-phase disturbance of the same frequency and wave number is superposed to the initial perturbation. In the ‘‘classical’’ case, frequency and wave number of both disturbances are the same. Looking at the wave numbers of the present example in Fig. 2(b) one can clearly see, that this is not the case here using the ω_z-control, because the wave number α_R and therefore the phase velocity c_{ph} of the controlled wave is strongly different from the uncontrolled case.

A deeper insight into the acting mechanisms can be obtained by looking at the spatial linear 2D energy balance

equation. This equation is derived from the 2D Navier–Stokes equations with the aid of a parallel flow assumption and a wave approach for the disturbances.[16,17] [Flow properties are split into steady mean and fluctuating quantities. Velocities in streamwise (x), wall normal (y) and spanwise (z) direction are $u=U+u'$, $v=V+v'$, $w=w'$, $\omega_Z=\Omega_z+\omega_z'$, respectively. Overlines denote the average over one period of time.]

$$E=\frac{d}{dx}\int_0^\infty \frac{1}{2}U(\overline{u'^2}+\overline{v'^2})dy$$
$$=R+D+P$$
$$\underbrace{-\nu\frac{d}{dx}\int_0^\infty \overline{v'\omega_z'}dy-\int_0^\infty(\overline{u'^2}-\overline{v'^2})\frac{\partial U}{\partial x}dy+\overline{v_w'p_w'}}_{\text{small}}, \tag{1}$$

where E is the spatial rate of increase of the fluctuation energy flux. $E>0$ indicates a growth of disturbances whereas $E<0$ means a weakening of disturbances.

The terms which form the major part of the right hand side of Eq. (1) are:

- the energy production term, where $\overline{u'v'}$ is the averaged Reynolds stress

$$R=\int_0^\infty -\overline{u'v'}\underbrace{\left(\frac{\partial U}{\partial y}\right)}_{>0}+\underbrace{\frac{\partial V}{\partial x}}_{\to 0}dy, \tag{2}$$

- the dissipation

$$D=-\nu\int_0^\infty \overline{\omega_z'^2}\,dy, \tag{3}$$

- and the pressure term

$$P=-\frac{1}{\rho}\frac{d}{dx}\int_0^\infty \overline{p'u'}\,dy. \tag{4}$$

All integrals are solved by integrating the flow quantities from the wall to the upper edge of the integration domain using finite differences of fifth-order accuracy. The error obtained by solving the integrals not to infinity is negligible because the integrands are already very close to zero at the upper boundary.

The application of ω_z-control at $x>2.5$ changes the sign of E together with the curves for R and P (Fig. 3). Clearly, the energy production term R dominates the complete energy balance. Its sign, respectively, the sign of the Reynolds stress $\overline{u'v'}$ [see Eq. (2)], determines the sign of the whole right-hand side of Eq. (1) and therefore the attenuation or growth of the regarded disturbance ($\overline{u'v'}>0\Rightarrow R<0\Rightarrow E<0\Rightarrow$reduction of amplitude and vice versa). The first of the two remaining terms, the dissipation term D has always a damping effect whereas the pressure term P always tends to counteract the production term R.

Normal-to-the-wall profiles of Reynolds stress, disturbance amplitudes and phases for a fixed x-position, for one case with amplification and the other with active damping, are shown in Fig. 4. The change of sign of the Reynolds stress $\overline{u'v'}$ [Figs. 4(a) and 4(d)] when control is applied is not caused by different u' or v' amplitudes [Figs. 4(b) and 4(e)] but by its strong sensitivity to the phase difference $\Delta\Theta=|\Theta(u')-\Theta(v')|$ around $\Delta\Theta(y)=\pi/2$ [Figs. 4(c) and 4(f)]. A phase difference of $\Delta\Theta(y)=\pi/2$ would lead to $\overline{u'v'}(y)=0$. Accordingly, a phase difference of $\Delta\Theta(y)<\pi/2$ results in positive Reynolds stress and damped disturbances in the controlled case, and vice versa. The effect of the control on the amplitude profiles is to increase v' at the wall to a finite value, leaving the profiles of u' and v' in the boundary layer more or less unchanged.

IV. LINEAR STABILITY THEORY

To get an overview of the damping capabilities of the new concept and to optimize the parameters for further simulations, investigations using linear stability theory (LST) were performed. Therefore, the boundary conditions at the wall for the Orr–Sommerfeld (and Squire equation) had to be changed (index w denotes wall properties) to

$$v_w'=A\cdot\omega_{z,w}'$$
$$v_w'=A\cdot\left(\frac{\partial u'}{\partial y}-\frac{\partial v'}{\partial x}\right), \tag{5}$$

$$(1+iA\alpha)\cdot v_w'-A\cdot\left(\frac{\partial}{\partial y}\right)_w u'=0 \tag{6}$$

with

$$A=|A|\cdot e^{i\Phi},$$

where $|A|$ is the amplitude factor and Φ is the phase difference between v_w and $\omega_{z,w}$ similar to the time delay used in the simulations. Due to the ability to express ω_z in terms of u and v [Eq. (6)] the discretized system remains a homogeneous eigenvalue problem which can be solved in the same way as the original Orr–Sommerfeld equation.

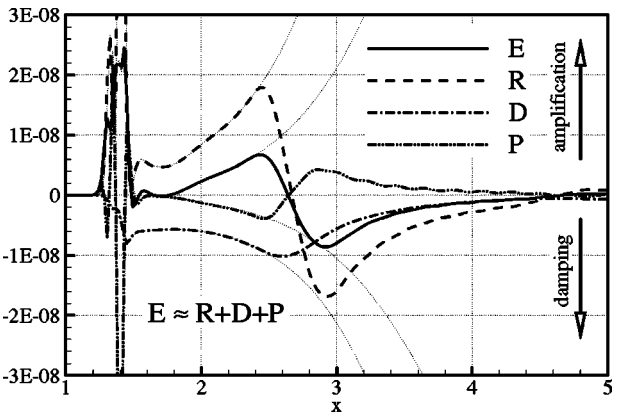

FIG. 3. Streamwise distribution of the main energy-balance terms based on Eq. (1), dotted lines: uncontrolled case for reference.

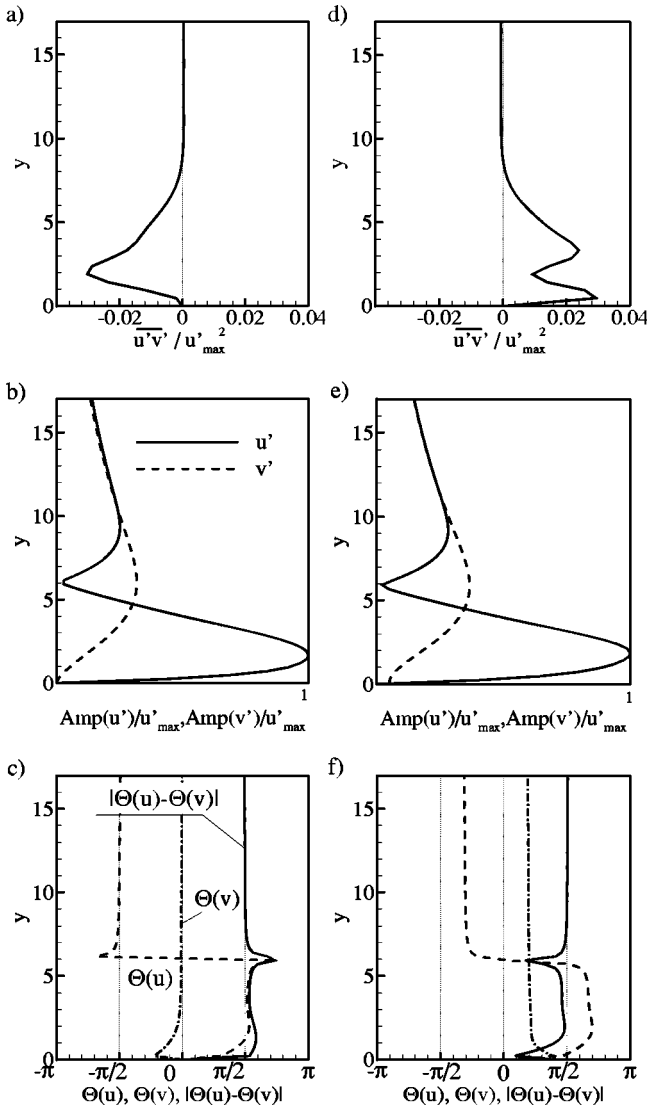

FIG. 4. Wall-normal distribution of Reynolds stress, amplitude of u' and v', phase and phase difference between both in the case of an amplified, uncontrolled (a–c) and actively damped Tollmien–Schlichting wave (d–f) at $x=3.0$ (same simulation as in Fig. 2 and Fig. 3).

A strong damping effect and a significant reduction of the unstable area in the stability diagram (Fig. 5) is already caused by very small amplitudes $|A|$.

Results of a detailed investigation of the influence on the most unstable eigenvalues are presented in Fig. 6 for amplitudes in the range of $5\times10^{-5}\leqslant|A|\leqslant20\times10^{-5}$ and all possible phase angles Φ between v_w and $\omega_{z,w}$. With increasing control amplitude the dependence of the spatial wave number α_R on the phase angle is changing from a sine-like curve to a curve with a singularity which strongly deviates from the uncontrolled case (Blasius). Two eigenvalues are shown for the largest amplitude $|A|$ because both are amplified for a certain region of Φ. Also they are no longer periodic with respect to Φ. However, when mode #1 leaves the domain at $\Phi=2\pi$ it has the same eigenvalues (α_r,α_I) as mode #2 at $\Phi=0$ which in turn exhibits the same values at $\Phi=2\pi$ as #1 at $\Phi=0$. This indicates that both belong to the same kind of disturbance which has now a 4π periodicity instead of the expected 2π. Similar results have been obtained by Sen and Arora[18] for the linear stability analysis of compliant walls. At $\Phi\approx\frac{3}{4}\pi$ α_R for $|A|=20\times10^{-5}$ tends to zero which causes problems for the local approach of LST so that the eigenvalues could not be computed there. For small to moderate control amplitudes the amplification rates indicate a 1:1 division of $\alpha_I>0$ and $\alpha_I<0$, i.e., damping and amplification (spatial approach of LST). Only the 4π periodic result is different. However, the large damping for $|A|=20\times10^{-5}$ of mode #1 for $\Phi<\pi$ has no particular advantage because of the existence of the unstable mode #2 which would amplify. Thus, the largest possible damping for all modes appears to the left of $\Phi\approx\pi/2$.

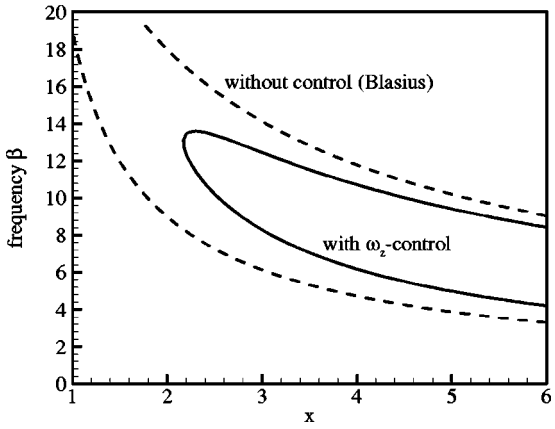

FIG. 5. Curve of zero amplification for 2D waves. Comparison of uncontrolled case (Blasius) and controlled case. Control parameters: $|A|=2\times10^{-5}$, $\Phi=0$.

After the influence of the control parameters on the eigenvalues have been investigated by LST, comparisons of some cases with results of DNS have been performed. One such example is shown in Fig. 7 where the spatial amplification rates of the simulation already discussed in the previous section are compared to the results obtained by linear stability theory. There is an excellent agreement between simulation and LST and the drastically reduced amplification is validated, as well as the influence of $|A|$ and Φ shown above.

V. ACTIVE CONTROL OF NONLINEAR DISTURBANCES

As a test case for the effect of the ω_z-approach on disturbances with large amplitude a typical K-breakdown scenario (dotted lines in Fig. 8) is used where a fundamental mode (1,0) with large amplitude and a stationary disturbance (0,1) (the first index denotes multiples of the fundamental frequency β, the second multiples of the basic spanwise wave number $\gamma=20$) are excited initially. Because of nonlinear interactions the 3D-mode (1,1) arises and falls in resonance with the fundamental 2D-mode (modes (1,0) and (1,1) share the same wave number from $x\approx3.4\ldots4.0$; cf. Fig. 9, dashed lines). The other modes shown are due to nonlinear combinations. They demonstrate transition to turbulence by generation of higher harmonics and the mean flow distortion (0,0). When the strongly amplified 3D-waves have reached

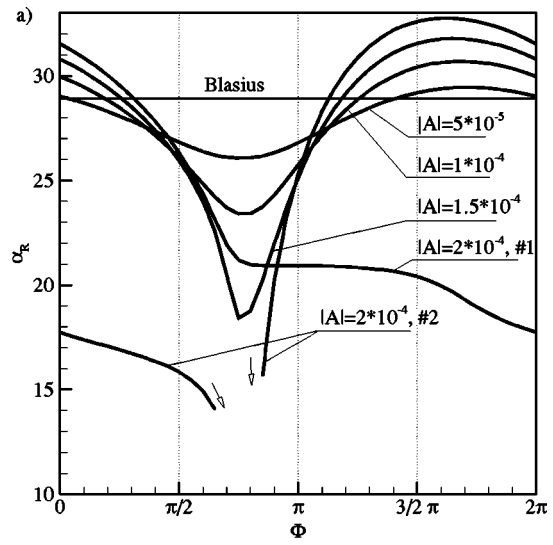

FIG. 6. Wave number α_R and amplification rate α_I from LST with ω_z-control ($v_w = |A| \cdot e^{i\Phi} \cdot \omega_{z,w}$) applied. Streamwise position: $x = 3.5$ ($\mathrm{Re}_{\delta 1} = 1018$), frequency: $\beta = 10$. (Note that for the spatial approach $\alpha_I < 0$ means amplification.)

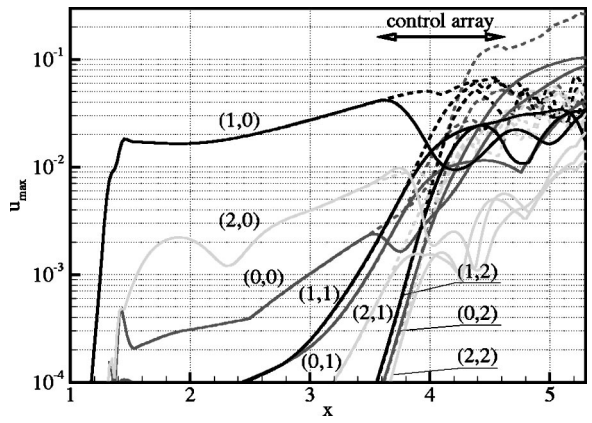

FIG. 8. K-breakdown, u_{max}-amplitudes vs x. Only 2D-modes controlled ($|A| = 2 \times 10^{-4}$, $\Phi \approx \pi/2$). Dashed lines: uncontrolled case; gray lines: higher harmonics.

the amplitude level of the fundamental mode, saturation sets in and transition to turbulence takes place (dashed lines). Applying ω_z-control to this scenario two main control effects can be distinguished: direct damping of nonlinear disturbances and the affection of the resonant behavior. The first is comparable to the linear case where ω_z-control was shown to be able to directly damp TS-disturbances.

In Fig. 8 only 2D modes, i.e., (1,0) and its higher harmonics were actively controlled with a phase Φ of approximately $\pi/2$ (control array from $x = 3.5$ to $x = 4.6$). Despite the strongly nonlinear regime in this case the amplitudes of the 2D modes (1,0) and (2,0) are strongly decreased.

The damping of the 3D-modes is now due to the second effect mentioned above: Resonance in 2D boundary layers is accompanied by phase synchronization of the resonant (1,1) to the fundamental (1,0) mode (i.e., both waves have the same phase speed $c = \beta/\alpha_{\mathrm{fundamental}}$). Investigations using LST predict apart from changed amplification rates strongly altered wave numbers of the controlled mode (Fig. 6). This effect leads to a decoupling of the resonant modes and can

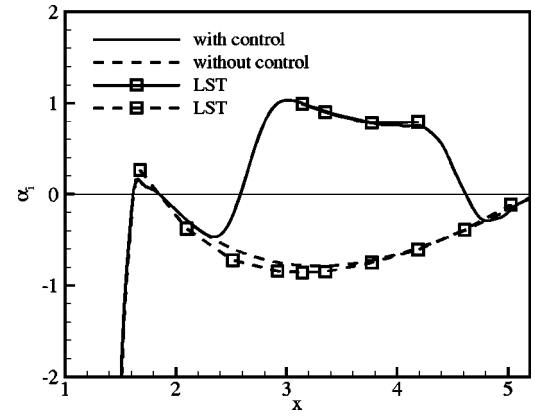

FIG. 7. Spatial amplification rates for a 2D TS wave with and without active control. Comparison of DNS and LST. Control parameters: $|A| = 7.5 \times 10^{-5}$, $\Phi = 0$, control array from $x = 2.4 \ldots 4.8$.

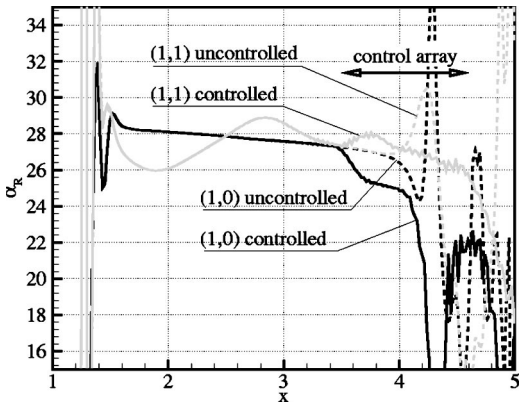

FIG. 9. K-breakdown, wave number α_R vs x. Only 2D-modes controlled ($|A| = 2 \times 10^{-4}$, $\Phi \approx \pi/2$). Dashed lines: uncontrolled case.

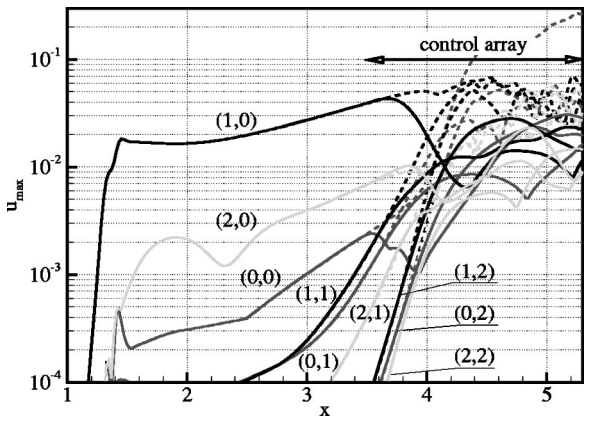

FIG. 10. K-breakdown, u_{max}-amplitudes vs x, active control of 2D modes (..,0) and modes with $\gamma=20$ (..,1) ($|A|=15\times10^{-5}$, $\Phi\approx\pi/2$). Dashed lines: uncontrolled case; gray lines: higher harmonics.

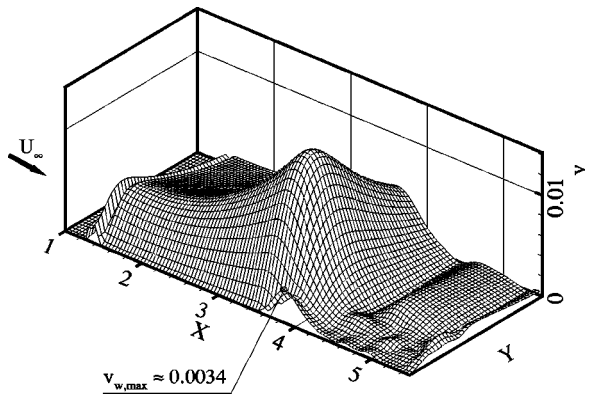

FIG. 12. v' amplitudes of the fundamental 2D-mode (1,0) for the controlled K-breakdown (see Fig. 10).

therefore suppress resonance. Figure 9 shows the wave numbers of the most important modes of the simulation mentioned above. Before the direct attenuation via ω_z-control can take effect the wave number of mode (1,0) is shifted to lower values (i.e., the wave is accelerated), the resonant mode (1,1) is not synchronized any more and resonance between (1,0) and (1,1) is prevented. Looking at further investigations applying ω_z-control in late nonlinear stages to both 2D and 3D modes an amplitude reduction of more than 50% is possible. Figure 10 shows a simulation with control of the 2D (..,0) *and* 3D (..,1) modes where the control array extends from $x=3.6$ to $x=5.5$. Compared to the previous simulations a further reduction of the disturbances is observed.

From the technological point of view the benefits in skin friction are of major interest. Figure 11 shows the local skin friction coefficient (dimensionless wall shear stress) c_f' of the simulation discussed above compared to the laminar and the uncontrolled case. Due to control skin friction close to the laminar state is reachable. Possible benefits in power requirement are difficult to quantify because the control result depends heavily on length, placement, and gain of the control strip. One hint for good efficiency may be that the control velocity v_w' in all cases shown in the present paper does not exceed a value of approximately 0.34% of the freestream velocity (Fig. 12). As an example we consider the pure skin friction of a flat plate with $\mathrm{Re}_l=500\,000$. Now it is possible to calculate the required ω_z-control input power, neglecting losses due to friction in tubes and valves:

$$P_{\mathrm{in}}=\frac{4}{3\pi}b\frac{\rho}{2}\int_{x1}^{x2}\hat{v}_w^3\,dx, \tag{7}$$

where b is the span, $\hat{v}_w$ is the amplitude of v at the wall and ρ is the density of air. The control array reaches from $\mathrm{Re}_{x1}=350\,000$ to $\mathrm{Re}_{x2}=500\,000$. Compared to the power savings ΔP due to reduced drag we obtain

$$\eta=\frac{P_{\mathrm{in}}}{\Delta P}=0.035. \tag{8}$$

That means that approximately 3.5% of the saved power has to be spent to drive the control actuators.

Flow structures. The effect of applying ω_z-control to the flow on the flow structures is discussed in the last two figures (Figs. 13 and 14). The ω_z-contours in Fig. 13 show a retarded development of high-shear layers compared to the uncontrolled (K-breakdown) case. In the uncontrolled case at $x\approx4.3$ the typical high-shear layer is followed by a rapid collapse which is absent in the controlled case. The remaining structures look more like longitudinal shear layers ac-

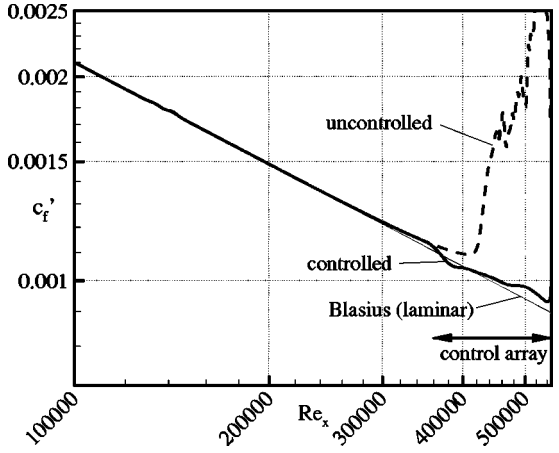

FIG. 11. Local friction coefficient for the controlled K-breakdown (Fig. 10). Dashed lines: uncontrolled case.

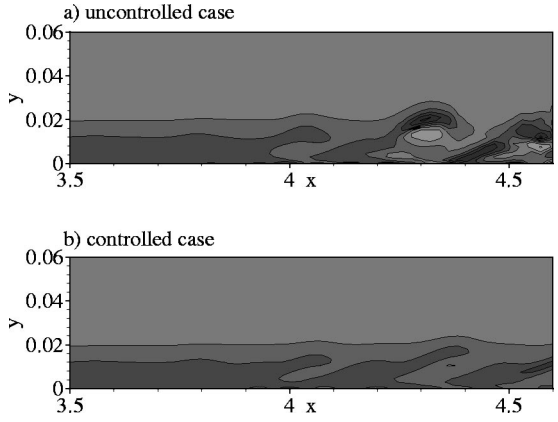

FIG. 13. K-breakdown, ω_z-contours in the peak plane ($z=0$), y-axis stretched by a factor of 5.

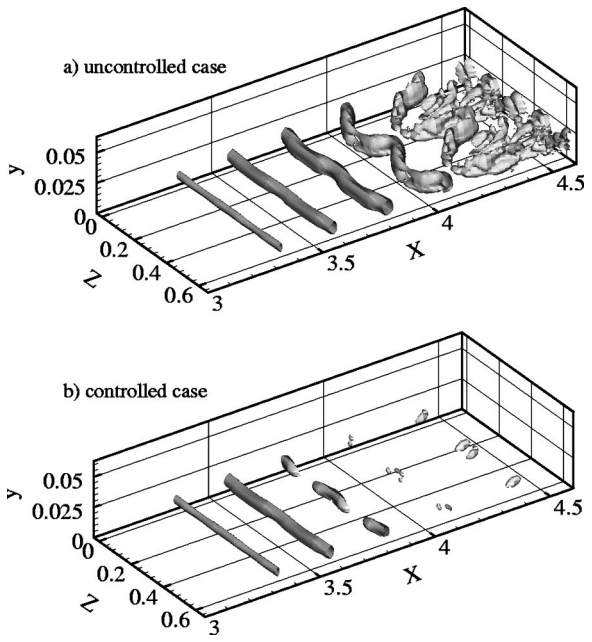

FIG. 14. Isosurfaces with $\lambda_2 = -15$, *y*-axis stretched by a factor of 5.

cording to the fact that the ω_z-control is only sensing instationary disturbances deviating from ω_z of the undisturbed base flow. Additionally, the λ_2 isosurfaces[19] in Fig. 14 indicate a complete suppression of transitional structures even in stages where the formation of Λ-vortices has already begun. The remaining structures show no significant amplification compared to the rapid nonlinear growth in the uncontrolled case.

VI. SUMMARY

With the aid of direct numerical simulations (DNS) it was possible to develop a simple, yet effective control algorithm to actively control the laminar-turbulent transition occurring in a 2D boundary layer. It combines two main effects: The direct attenuation caused by a change of the energy properties and a reduced resonance according to an altered phase velocity of the involved modes. Calculations using linear stability theory (LST) show a strong dependence of the resulting wave number and amplification rate on the chosen amplitude and phase difference between ω_z' (sensed) and v'_{wall} (stimulated).

It is shown that this approach works very well even close to transition where the boundary layer instabilities have reached a highly nonlinear stage. Further investigations have to show how far transition can be shifted downstream and whether a complete relaminarisation of the flow is possible using this approach.

ACKNOWLEDGMENT

The support of this research by the Deutsche Forschungsgemeinschaft DFG is gratefully acknowledged.

[1] R. W. Milling, ''Tollmien–Schlichting wave cancellation,'' Phys. Fluids **24**, 979 (1981).
[2] H. W. Liepmann, G. L. Brown, and D. M. Nosenchuck, ''Control of laminar-instability waves using a new technique,'' J. Fluid Mech. **118**, 187 (1982).
[3] H. W. Liepmann and D. M. Nosenchuck, ''Active control of laminar-turbulent transition,'' J. Fluid Mech. **118**, 201 (1982).
[4] V. V. Kozlov and V. Y. Levchenko, ''Laminar-turbulent transition control by localized disturbances,'' in *Turbulence Management and Relaminarization*, IUTAM-Symposium, Bangalore, India, 1987, edited by H. W. Liepmann and R. Narasimha (Springer Verlag, Berlin, 1987).
[5] M. Baumann and W. Nitsche, ''Investigations of active control of Tollmien–Schlichting waves on a wing,'' in *Transitional Boundary Layers in Aeronautics*, edited by R. A. W. M. Henkes and J. L. van Ingen (North Holland, Amsterdam, 1996), Vol. 46, pp. 89–98.
[6] E. Laurien and L. Kleiser, ''Numerical simulation of boundary-layer transition and transition control,'' J. Fluid Mech. **199**, 403 (1989).
[7] P. Koumoutsakos, ''Active control of vortex–wall interactions,'' Phys. Fluids **9**, 3808 (1997).
[8] P. Koumoutsakos, T. R. Bewley, E. P. Hammond, and P. Moin, ''Feedback algorithms for turbulence control—Some recent developments,'' AIAA **97**, 2008 (1997).
[9] H. Choi, P. Moin, and J. Kim, ''Active turbulence control for drag reduction in wall-bounded flows,'' J. Fluid Mech. **262**, 75 (1994).
[10] M. Baumann, D. Sturzebecher, and W. Nitsche, ''On active control of boundary layer instabilities on a wing,'' in *Notes on Numerical Fluid Mechanics*, edited by W. Nitsche, H. J. Heinemann, and R. Hilbig (Vieweg-Verlag, Braunschweig, 1998), Vol. 72, pp. 22–29.
[11] S. S. Joshi, J. L. Speyer, and J. Kim, ''A system theory approach to the feedback stabilization of infinitesimal and finite-amplitude disturbances in plane Poiseuille flow,'' J. Fluid Mech. **332**, 157 (1997).
[12] H. H. Hu and H. H. Bau, ''Feedback control to delay or advance linear loss of stability in planar Poiseulle flow,'' Proc. R. Soc. London **447**, 299 (1994).
[13] M. Kloker, ''Direkte Numerische Simulation des laminar-turbulenten Strömungsumschlages in einer stark verzögerten Grenzschicht,'' Dissertation, Universität Stuttgart, 1993.
[14] U. Konzelmann, ''Numerische Untersuchungen zur räumlichen Entwicklung dreidimensionaler Wellenpakete in einer Plattengrenzschicht,'' Dissertation, Universität Stuttgart, 1990.
[15] U. Rist and H. Fasel, ''Direct numerical simulation of controlled transition in a flat-plate boundary layer,'' J. Fluid Mech. **298**, 211 (1995).
[16] F. R. Hama, D. R. Williams, and H. Fasel, ''Flow field and energy balance according to the spatial linear stability theory of the Blasius boundary layer,'' in *Laminar-Turbulent Transition*, IUTAM Symposium Stuttgart/Germany, 1979 (Springer-Verlag, Berlin, 1980).
[17] F. R. Hama and S. de la Veaux, ''Energy balance equations in the spatial stability analysis of boundary layers with and without parallel-flow approximation,'' Princeton University, Princeton, New Jersey, 1980.
[18] P. K. Sen and D. S. Arora, ''On the stability of laminar boundary-layer flow over a flat plate with a compliant surface,'' J. Fluid Mech. **197**, 201 (1988).
[19] J. Jeong and F. Hussain, ''On the identification of a vortex,'' J. Fluid Mech. **285**, 69 (1995).